PCCP

Accepted Manuscript

ROYAL SOCIETY OF CHEMISTRY

www.rsc.org/pccp

Journal Name

ARTICLE

Electronic defect states at the $LaAlO_3/SrTiO_3$ heterointerface revealed by O K-edge X - ray absorption spectroscopy

Received 00th January 20xx,
Accepted 00th January 20xx

DOI: 10.1039/x0xx00000x

www.rsc.org/

Natalia Palina[a,b,†], Anil Annadi[b,e], Teguh Citra Asmara[a,b,c], Caozheng Diao[a], Xiaojiang Yu[a], Mark B. H Breese[a,c], T. Venkatesan[b,c,d], Ariando[b,c,†], Andrivo Rusydi[a,b,c,†]

Interfaces of two dissimilar complex oxides exhibit exotic physical properties that are absent in their parent compounds. Of particular interest is insulating $LaAlO_3$ films on insulating $SrTiO_3$ substrate, where transport measurements have shown a metal-insulator transition as a function of $LaAlO_3$ thickness. Their origin has become the subject of intense research, yet a unifying consensus remains elusive. Here, we report evidence for the electronic reconstruction in both insulating and conducting $LaAlO_3/SrTiO_3$ heterointerfaces revealed by O K-edge X-ray absorption spectroscopy. For the insulating samples, the O K-edge XAS spectrum exhibits features characteristic of electronically active point defects identified as noninteger valence states of Ti. For conducting samples, a new shape-resonance at ~540.5 eV, characteristic of molecular-like oxygen (empty O-2p band), is observed. This implies that the concentration of electronic defects has increased in proportion with $LaAlO_3$ thickness. For larger defect concentrations, the electronic defect states are no longer localized at the Ti orbitals and exhibits pronaunced O 2p-O 2p character. Our results demonstrate that, above critical thickness, the delocalization of O 2p electronic states can be linked to the presence of oxigen vacanciea and is responsible for the enhancement of the conductivity in at the oxide heterointerfaces.

Introduction

Interfaces between perovskite oxides (ABO_3) can exhibit a wide range of exotic properties such as two-dimensional electron gas (2DEG) [1], magnetism [2-4] and superconductivity [5, 6], which are absent in the bulk constituent. Ever since the discovery of the 2DEG at the interface between insulating $LaAlO_3$ (LAO) and $SrTiO_3$ (STO) [1], its origin has been a source of considerable debate. LAO thickness dependent metal-insulator transition is still most intriguing property of the LAO/STO system. For the case of TiO_2 terminated (001) STO substrate transport measurements have shown that the 2DEG appears for a LAO layer above a critical thickness of four unit cell (4 u.c.), below which the interface remains insulating [7]. This has been exploited successfully to create nanoscale devices using c-AFM lithography and selective deposition processes [8-9], and eventually led to the study of many quantum phenomena. Formation of centers of instability at surfaces and interfaces such as: (i) lattice distortion and/or chemical defects close to the heterointerface [10–12], (ii) cation substitution and/or intermixing [13], (iii) formation of oxygen vacancies (Vo) at either LAO surface [14] or STO interface [15, 16] and (iv) electronic reconstruction, e.g. charge transfer [17] have been proposed to explain the observed 2DEG.

Based on the experimental data published thus far, electronic structures of the metal and insulator cases at the LAO/STO interface are not fully understood. For the conducting case, an oxygen vacancies hypothesis is supported by experimental techniques such as cathode and photoluminescence experiments [16] and high-energy optical conductivity [14]. For insulating samples, the application of techniques utilizing electrons or X-ray for excitation and detection of the signal is challenged mostly by the charging effect. The charging effect influences the energies of detected electrons and hence causes shifts of features in X-ray photoemission spectroscopy (XPS) and Auger electron spectroscopy (AES) [18]. However, for X-ray absorption near-edge structure (XANES) technique, the energy is defined by the incident radiation and so the effect of charging will not cause shifts of spectral features even if the signal is collected using the total-electron-yield mode (TEY) [19, 20].

[a] Singapore Synchrotron Light Source, National University of Singapore, Singapore 117603, Singapore.
[b] NUSNNI-Nanocore, National University of Singapore, Singapore 117411, Singapore.
[c] Department of Physics, National University of Singapore, Singapore 117542, Singapore.
[d] Department of Electrical and Computer Engineering, National University of Singapore, Singapore 117576, Singapore
[e] Department of Physics and Astronomy, University of Pittsburgh, Pittsburgh, Pennsylvania, 15260, USA
† natalie.mueller@nus.edu.sg, phyarian@nus.edu.sg, phyandri@nus.edu.sg.
Electronic Supplementary Information (ESI) available: [LAO_ESI_NM.pdf]. See DOI: 10.1039/x0xx00000x

In this letter we focus on the oxygen K–edge XANES analysis in order to differentiate driving forces behind electronic and/or structural reconstruction at the 1 u.c. (as a model system for insulating) and 5 u.c. (as a model system for conducting) LAO/STO heterointerfaces. X-ray absorption, in general, is an element- and symmetry-selective process with a high surface sensitivity, which makes it suitable for (ultra) thin film analysis such as in the present work. Here we are attempting to emphasise an importance of a thorough investigation of oxygen K–edge XANES spectra. The unique value of O K–edge XANES analysis originates from the fact that transitions from oxygen 1s states directly reflect the oxygen p-projected unoccupied density of states and hence probe the nature of covalent mixing (hybridization) between metal and oxygen states. Another advantage of oxygen K–edge XANES analysis lays in the possibility to obtain electronic information on an unknown sample based on comparison with an accurate set of suitable reference compounds. This approach is so-called 'fingerprint' analysis. It can be extremely useful, as it provides information often not otherwise accessible. XANES analysis is also sensitive to identify integer and noninteger electronic valences of elements as an energy position of spectral features, hereafter shape-resonances, strongly depend on the electronic overlap between central and bonding atoms.

Experimental

Sample preparation

The LAO/STO samples were prepared using Pulsed Laser Deposition by ablating LAO target onto the TiO_2 terminated single crystal STO (100) substrates. The LAO unit cell layer number was precisely controlled by monitoring the in situ-RHEED during the growth. The growth conditions employed for these samples are similar to the previous reports [2, 14]. Deposition conditions ensure fabrication of films with minimal reacting effects such as surface sputtering and chemical reactivity on the substrate surfaces. Along with the RHEED patterns of LAO growth the XRD and TEM characterisation of films are usually performed. XRD confirms the epitaxial growth of single phase LAO film on STO. TEM micrograph confirms the growth of LAO phase and a sharp interface of LAO/STO. XRD and TEM data are available in ESI†. LAO films with a thickness of 1 u.c, 3 u.c, 4 u.c. and 5 u.c. was studied in this work. The layer by layer growth of LAO layers also ensures the sample surface roughness and is in the order of sub unit cell at these LAO thicknesses.

Electrical conductivity measurements

To examine the electrical conductivity of LAO/STO samples, electrical measurements were carried out at room temperature. The samples showed a LAO layer thickness dependent metal–insulator transition at about 4 unit cells (i.e. 1 and 3 unit cells of LAO on STO are insulating, and 4 and 5 unit cells are conducting). All samples showed comparable basic characteristics similar to those previously reported elsewhere [2, 12, 14].

X-ray absorption near-edge structure measurements (XANES)

The XANES spectra were collected at the SINS beam-line at the Singapore Synchrotron Light Source (SSLS), using spherical gratings in a modified dragon-type monochromator with overall resolution at oxygen K- edge of about 0.4 eV [21]. For O K–edge XANES spectra acquisition the photon energy was varied from 525 to 570 eV. All XANES spectra were acquired in UHV chamber with a background pressure of about $2x10^{-10}$ mbar. All data presented here were recorded *ex-situ* and at X-ray incident angle of 90° using total electron yield (TEY) mode. Recorded spectra were normalized to beam current measured by a gold mesh in front of sample, to correct for synchrotron intensity decay during spectra acquisition. The high heterointerface sensitivity is achieved by combination of the X-ray incident angle geometry and relatively low kinetic energy of the detected electrons. Although the X-ray photons penetrate many microns deep into the sample, the electrons generated at that depth do not emerge from the sample. The effective escape depth, and therefore the information depth of electron yield XANES, has been estimated to be in the range of 3-5 nm for metals and semiconductors, and slightly larger for insulators (5-10 nm) due to reduced electron–electron scattering [18, 22]. Least squares linear combination fitting (LCF) was used to identify origin of shape-resonances present in each sample by fitting each sample spectrum with weighted mixtures of the principal compounds. The LCF analysis of XANES spectra for insulating and conducting samples suggests presence of unique states in both samples, which are not present in pristine principal compounds and hence attributed to changes at the heterointerface.

X-ray photoemission spectroscopy (XPS)

The XPS spectra were recorded at room temperature and *ex-situ* at the SINS beam-line at the Singapore Synchrotron Light Source (SSLS). The incident photon energy was 850 eV and 455 eV for core-level (CL) and resonant valence band (VB) measurements, respectively. The exit slit width was set at 100 μm, resulting with photon flux of about ~$2x10^{10}s^{-1}$/100mA. For all XPS measurements the energy resolutions was better than 0.6 eV. Spectra were collected with an Omicron EA 125 hemisphere energy analyzer equipped with 7 channeltron electron multipliers. The pass energy was set to 50 eV and 20 eV for CL and VB measurements respectively. The energy scale was calibrated against the Au $4f_{7/2}$ peak at 84.00 ±0.05 eV using an Au foil. All samples were mounted on carbon tape. As insulating samples are suffering from surface charging effects during XPS measurements, respective spectra were shifted to align with the energy of carbon 1s spectrum (peak at 285 eV) obtained for conducting sample. We want to emphasise that even though CL C 1s peak was present in all samples, it not compromising current interpretation of the XANES data. Note, that experimental O K–edge XANES spectrum of bulk STO used in this study, with carbon adsorption, shows no (i) "misleading

structure in the O K–edge XAS spectra", (ii) broadening of spectral features or (iii) noticeable change in the energy position of main peaks as compared to either calculation [23] or previously reported experimental data [25]. For details, please refer to ESI† (Figure ESI 2). Therefore, we conclude that in our analysis changes observed in O K–edge XANES are originated from the thickness dependent changes at the interface.

Results

The XANES spectra of insulating 1 u.c. (black) and conducting 5 u.c. (red) LAO/STO samples along with reference spectra of pristine STO (pSTO, triangle scatters), TiO_2 terminated STO (tSTO, square scatters) and LAO (circle scatters) are shown in Figure 1 (spectra of 3 u.c. and 4 u.c LAO/STO samples are available in the ESI† (Figure ESI 8)). For complex metal oxides, the O K–edge energy region can be divided into two regimes. The first regime, is defined as the low–energy range and of about 10 eV from the absorption edge, covers energies from 525 to 539 eV. Compared to references, shape–resonances in low–energy regime arise from two main transitions: (i) from O 1s $\rightarrow$ to hybridized O 2p $\Leftrightarrow$ Ti 3d (Al 3p), see peaks A, B (G), and (ii) from O 1s $\rightarrow$ to hybridized O 2p $\Leftrightarrow$ Sr 4d (La 5d) transitions, refer to peaks C, D and (H, J) in Figure 1. The four shape–resonances labelled as A, B and C, D are reflecting split of main transition (i) and (ii) into t_{2g} and e_g levels due to crystal field effect. As Al 3p states are not affected by crystal field splitting, the XANES spectrum for the LAO reference compound exhibits only three pronounced shape-resonances in that energy region (refer to peaks G–J). The second regime is the high–energy range extending from 539 to 560 eV. The high–energy range is dominated by broad shape–resonance features corresponding to transitions into hybridized metal–oxygen orbitals involving Ti 4sp/La 6sp (refer to peaks E and L), respectively. Assignment of O K–edge XANES resonance transitions is in a good agreement with available calculations for bulk pSTO [23] and LAO [24]. Experimental O K–edge XANES spectra of reference bulk LAO and bulk pSTO presented here are also consistent with experimental data published by other groups [3, 23, 25]. Summary of the energy position for main resonance transitions are shown in ESI†.

Comparison of XANES spectra for insulating and conducting LAO/STO samples reveals that the intensity and number well pronounced shape-resonances and their peak positions are notably different. Observed difference are originated from: (i) the fact that the absorption spectrum of LAO/STO is a superposition of LAO and STO principle compounds, (ii) defect-induced changes that might be present at the LAO/STO heterointerface. First argument is evident comparing 5 u.c. (1 u.c.) LAO/STO XANES spectrum, having a larger (smaller) LAO weight, to LAO (tSTO) reference spectrum. Even though, the overall shape of 1 u.c. and 5 u.c. LAO/STO spectra resembles tSTO and LAO references, respectively, clear differences (compared to references and each other) are observed in the high-energy regime.

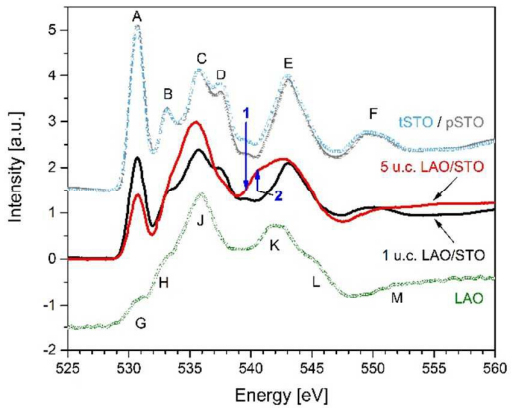

Fig. 1. XANES spectra of insulating 1 u.c. (black) and conducting 5 u.c. (red) LaAlO3/SrTiO3 (LAO/STO) samples along with reference spectra of bulk pristine and TiO2-teminated STO (pSTO triangle scatters and tSTO square scatters) and LAO (circle scatters).

For an insulating sample, the intensity of peak 1 at the energy position around 539.6 eV is higher compared to the pristine STO (pSTO) and TiO_2 terminated STO (tSTO) reference sample. We are attributing this change to be indicative to the formation of electronically active defects at the LAO/STO heterointerface. For a conducting sample, a unique electronic states are observed at the energy of 540.5 eV (peak 2), which is not observed in principle compounds. For more details see 2nd derivative of XANES spectra in Figure 2. Here we argue that for LAO thicknesses above critical, spectral changes in the high-energy regime are reflecting defects-induced electron correlation between film and substrate and can be attributed to a reconstructed heterointerface electronic structure. These findings will be discussed in details below.

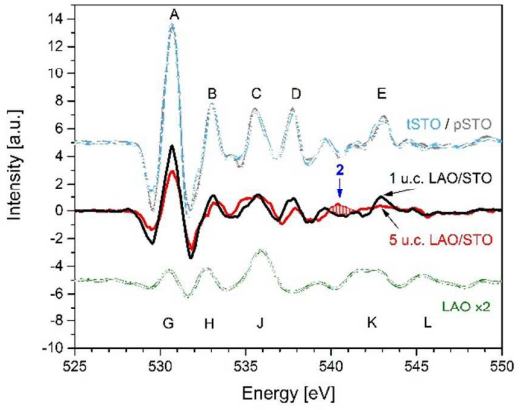

Fig. 2. Second order derivative of XANES spectra. Peak 2 (540.5 eV), observed for conducting LAO/STO sample is shadowed. Reference compounds do not exhibit peak in

the energy range at or around 540.5eV. Therefore, we are attributing peak 2 to be a characteristic to defects-induced electronic reconstruction at heterointerface, e.g. formation of 2DEG.

Discussion

TiO_2 terminated STO and insulating LAO/STO sample

The defect-induced phenomena cannot be ignored in understanding thickness dependent changes in the physical properties of LAO/STO system. Let's turn to a possible influence of the substrate at first. In this work, the atomically smooth TiO_2 termination was obtained by treating the crystal surface with a pH-controlled NH_4F-HF buffer solution and subsequent anneal in O_2 atmosphere [26-28]. Even though this procedure is well known and widely used, we find a non-negligible change in the electronic properties comparing pristine and TiO_2 terminated substrates, pSTO and tSTO respectively. Spectral changes that are illustrative to modification in the electronic states can be traced as difference in the intensity of peak D and peak 1, see Figure 1. For both peaks, an intensity is higher for tSTO compared to pSTO substrates. Slight increase in the intensity of peak D could be related to the presence of Sr adatoms and/or SrO as previously reported elsewhere [29, 30]. Note that the presence of Sr adatoms and/or SrO is also supported by XPS study (the CL XPS spectra and ration of Sr/Ti atoms for tSTO vs pSTO are available in the ESI† (Figure ESI 3)). In Figure 1, peaks A and B probe directly O 2p and Ti 3d hybridyzation and their intensity is not changing drastically for pSTO and tSTO, suggesting that chemical treatment results in more or less constant number of chemically modified Ti–O bonds. Additionally, the Ti–O bond is much stronger than Ti–Ti bonds and O–O bonds. Changes in O–O and Ti–Ti are more sensitive. First manifests itself as an increased intensity of peak 1, probing O2p–O2p bond. And later is shown in the ESI† (Figure ESI 6(a), note increase intensities of valleys 1 and 2 for tSTO compared to pSTO)).

At this point, we are suggesting that a noticeable increase in the intensity of peak 1 (539.6 eV) is indicative to the formation of electronically active defects at the tSTO surface. A most probable origin of electronically active defects is presence of Ti ions with noninteger valence states e.g. $Ti^{(4-x)+}$, where $0 < x < 1$. It is no different to involuntary accumulation of negative charge, e.g. electron doping similar to what previously reported as unintentional F doping [31]. The origin of extra electrons may be due to breaking of Sr–O bond which leads to the escape of O^- ions and theirs consequent trapping at Ti 3d orbitals. When a host Ti^{4+} ion is changed to Ti^{3+} or noninteger valence state ion, the local electrostatic balance is broken. A change in the O 2p–O 2p bond strength is introduced to compensate for the charge difference. This change can be traced by analysis of O K–edge XANES spectra of reference compounds representing tetravalent and trivalent Ti ions, see Figure 3. Calculations and previously reported experimental data [23, 32], show that for bulk TiO_2 O 2p–O 2p states appear at about 12 eV from the onset of the absorption edge. In Figure 3, these shape–resonances are marked as 1′ and 1′′ for TiO_2 (open triangular scatters) and Ti_2O_3 (solid square scatters) reference compounds [33], respectively. As can be seen, the peak position varies inversely with the O 2p–O 2p bond strength, indicating stronger orbital overlap for TiO_2 (538.8 eV) as compared to Ti_2O_3 (540 eV).

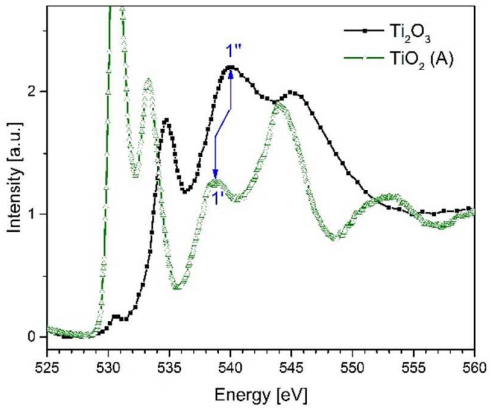

Fig. 3. XANES references of TiO_2 (anatase, open triangular scatters) and Ti_2O_3 (filled square scatters), reproduced with permission [33].

In XANES spectra of reference pSTO and tSTO, the position of peak 1 is, thus related to the O 2p–O 2p bond strength. For pSTO and tSTO, peak 1 appears at the energy of 539.6 eV at about 10.6 eV from the onset of the O K–edge absorption edge (529 eV, see Figure 2). Energy position of peak 1 corresponds to convolution of energy positions of peaks 1′ and 1′′ of titanium oxide references and suggests presence of noninteger valence states for Ti ions, e.g. electronically active defects localized at Ti orbitals. Note that even though tSTO can be regarded as electronically modified, it remains insulating. FWHM of main spectral features recorded for pSTO and tSTO shows no observable broadening and hence support scenario of localized charge accumulation at Ti site. Otherwise, the presence of oxygen defects, e.g. delocalized electrons, should have resulted in the broadening of O K–edge XANES shape–resonances due to reduced lifetime in the resonant process and disorder in the local coordination.

To further support this statement, we performed a fitting procedure to reproduce the experimental spectrum by a least squares linear combination fitting (LCF) of reference compounds. Figure 4 compares data for the insulating sample (solid line) with a LCF spectra (dashed line). The latter is obtained by appropriately combining the measured XANES of LAO and STO references, shown in Figure 1. As can be seen, the LCF based on the tSTO and LAO references does not show any appreciable difference compared to experimental data except for one shape-resonance, namely peak 1. On the other hand, the LCF which includes a weighted contribution from Ti_3O_5, where Ti ions are present at mixed (noninteger) valence state (see (Figure 4, dotted line) reproduced the intensity of the peak 1 more accurately. Please note, that in all compounds

used for LCF Ti is in octahedral coordination and all reference compounds are bulk and insulating in nature, cause no contradiction in the observed conducting behaviour of 1 u.c. LAO/STO sample shown in Figure 4. For bulk Ti_3O_5 metallic conductivity has been observed at temperatures above 460 K [34, 35]. All XANES data shown here are acquired at RT (300 K).

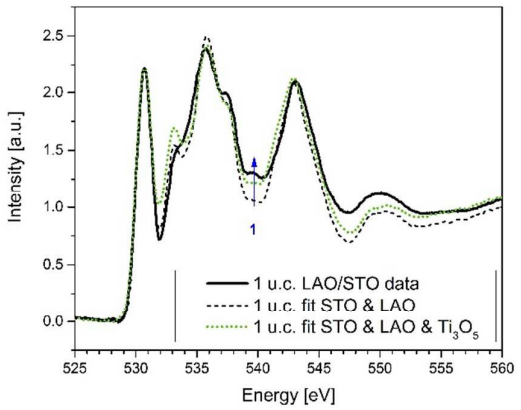

Fig. 4. XANES spectrum of 1 u.c. $LaAlO_3/SrTiO_3$ (LAO/STO) sample (solid line) with corresponding best linear combination fit based on the LAO and pSTO references (dashed line) and including Ti3O5 reference (dotted line).

And lastly, presence of localized electronically active defects is also supported by resonant valence-band XPS study of pSTO and tSTO references as shown in the Figure 5. This observation is in accordance with previously reported data [31]. In XPS study, density of states which attributed to electronically active defects appears at the bottom of the valence band, at about 11 eV in perfect agreement with position of peak 1 in XANES data.

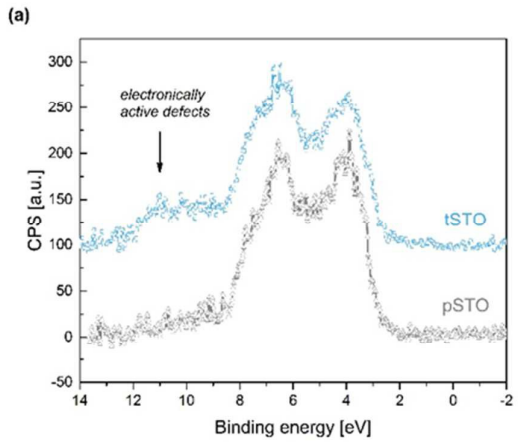

Fig. 5. Normal emission resonant valence band XPS spectra (hv=455 eV) for the pristine STO (pSTO triangle scatters) and TiO_2 terminated STO (tSTO, square scatters). The electronically active defects appeared at the bottom of the valence band, around 11 eV.

Therefore, our data reveals that TiO_2 termination of pSTO with NH_4F-HF buffer solution results in non-negligible changes in the electronic structure, namely accumulation of negative charge at the terminated surface which is localized at Ti 3d orbitals. These electronically active defects are identified as Ti ions with noninteger valence states e.g. $Ti^{(4-x)+}$, where $0 < x < 1$. XRD and TEM data shows that chemical reduction of TiO_2 will not cause formation of different crystallographic phase. Here we also want to point out that TiO_2-termination of STO substrate alone is not enough to promote conductivity in the STO substrate.

Based on the information above, O K–edge spectrum of insulating LAO/STO sample can be compared to tSTO in a following manner: (i) overall reduction of shape-resonances intensity (peaks A-F) is caused by the attenuation of X-ray signal due to LAO deposition, (ii) no broadening of shape-resonances indicates that all charge is localized at Ti orbitals and (iii) an increased intensity of peak 1, manifests a release of accumulated negative charge from the electronically active defects (Ti ions with noninteger valence state) at heterointerface. We suggest that for the insulating LAO/STO sample charge neutrality achieved by charge transfer (from polar LAO into heterointerface) and electronic reconstruction at the heterointerface caused by covalent bond formation between LaO and TiO2 layers resulting in charge redistribution at the heterointerface (note an increased intensity of La M_5 edge shown in ESI† (Figure 6 (b)). Additionally, a release of accumulated negative charge presented at electronically active defects is observed as an increase of peak 1 intensity. Reconstruction manifests itself mainly as charge redistribution between LAO and O 2p and Ti $^{4+}$ as well as defect-induced Ti $^{(4-x)+}$ orbitals. At these orbitals electrons are localized and have no mobility, explaining the insulating nature of 1 u.c. LAO/STO sample. This scenario is also energetically more favourable compared to atomic reconstruction and cationic substitution. To illustrate the specific orbital involvement, we also measured XLD signal. As can be seen in Figure 7, for insulating sample main contribution to resulting XLD signal originated from Ti 3d orbitals, both t_{2g} and e_g, and defect-induced Ti $^{(4-x)+}$ states, see shaded area at the energy position of peak 1. These findings provide additional support to the above mentioned conclusion. Additionally, O K–edge XANES shows no direct evidence for either cationic displacement or atomic reconstruction (buckling) as the position of the shape–resonances are identical between the pSTO, tSTO and 1 u.c. LAO/STO samples.

Conducting LAO/STO sample

Comparing to insulating LAO/STO XANES spectrum, spectral features of XANES obtained for conducting LAO/STO sample (Figure 1) can be understood as following: (i) overall reduction of shape-resonances intensities characteristic for Ti 3d and Sr 4d transitions is caused by the attenuation of X-ray signal due to increased LAO thickness. Remarkably, (ii) no shape-resonance is observed at the energy of 539.6 eV (peak 1), indicating that with increased thickness of LAO, sites assigned

to localized electronically active defects are fully populated, see Figure 6 (b). This implies that charge redistribution between LaO and TiO2 layers is still in place and concentration of electronic defects increased proportionally with $LaAlO_3$ thickness. The remaining fraction of electrons contributing to the charge redistribution between LAO and STO is responsible for 2DEG formation. And (iii) presence of defects-induced electronic reconstruction at the heterointerface, which manifests itself by appearance of new shape-resonance at ~540.5 eV (peak 2). Energy position as well as broadening of spectral features suggests formation of oxygen vacancies. This argument is further supported by LFC procedure. As can be seen in Figure 6 (a), a LCF based either on LAO and STO (dashed line) or including contribution from Ti_3O_5 (not shown) failed to match the experimental data. A LCF represents the formation of a hypothetical interface, which does not include effects of electronic correlation and/or defect-induced changes, e.g. carriers are localized at the respective orbitals as in reference compounds. That is why shape-resonance at about 540.5 eV (peak 2) associated with the formation of the 2DEG (pronounced O 2p–O 2p interactions) at the heterointerface cannot be reproduced by this procedure. LCF also doesn't accounts for collective interactions of electrons, extending to either sides of heterointerface. Hence, the shape-resonance at about 535eV is not reproduced accurately.

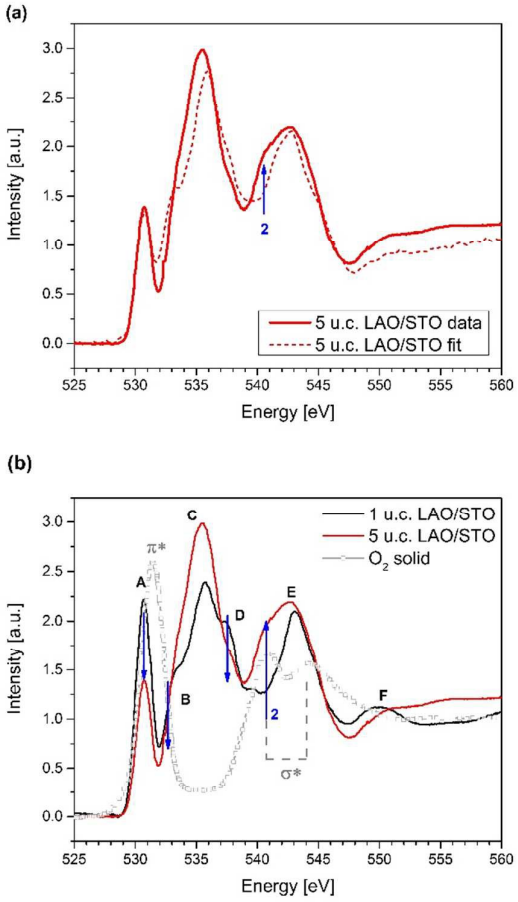

Fig. 6. (a)]XANES spectrum of 5 u.c. LAO/STO sample with corresponding best linear combination fit (solid and dashed lines, respectively **(b)** Thickness dependence comparison of the LAO/STO XANES spectra with references O K-edge XANES spectra of solid O_2 (square scatters), reproduced with permission [36].

Note that collective interactions of electrons involving Ti/Sr/La states, can be clearly traced by examining XLD signal, shown in Figure 7. The shape-resonance at about 540.5 eV (peak 2) is thus a unique feature indicating pronounced O 2p–O 2p interactions (formation of oxygen vacancies) observed only for LAO thickness above critical. To emphasise a unique nature of peak 2, e.g. having mostly O 2p–O 2p interactions character, we show the O K–edge XANES spectrum of molecular oxygen, see triangular scatters in Figure 6 (b). For conducting LAO/STO, the position of peak 2 well matches the position of the σ* peak observed in the molecular-like oxygen spectrum. Note that despite a clear broadening observed with increased LAO thickness for shape-resonance at about 544 eV, an energy position of peak 2 is different from main peaks (K and L) of LAO reference compound (see ESI† Figure 7 for details). Hence, we argue that 5 u.c. LAO/STO is a strongly correlated electron system where carriers are delocalized. Observed defect-induced phenomenon is likely to be linked to a presence of oxygen vacancies and supports scenario of electronic reconstruction at the heterointerface for the LAO thickness above critical.

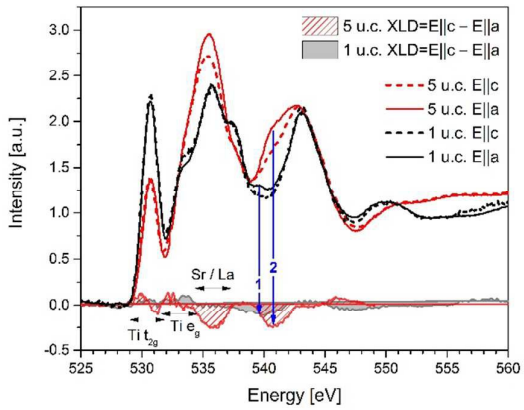

Fig. 7. Thickness dependence O K-edge XLD signals (shadowed areas) for the insulating (black) and conducting (red) LAO/STO samples.

By combining information observed from recent high-energy optical conductivity measurements reported elsewhere [14], we propose an electronic band structure for insulating and conducting samples as shown in Figures 8 (c) and Figure 8 (d), respectively. The electronic band structure of insulating bulk STO is well-known and consists of a fully occupied O 2p band forming the highest valence band and the empty Ti 3d band forming the lowest conduction band. In insulating LAO/STO, the presence of extra electrons at the interface are localized at

the Ti 3d band and split later into two Hubbard-like bands as large as 3-4 eV. This statement is also supported by recently published spectroscopic ellipsometry study on $SrTiO_3$ and $SrTi_{1-x}Nb_xO_3$ [37]. In conducting LAO/STO, the density of the extra electrons is higher compared to an insulating sample, resulting in charge redistribution between Ti 3d Hubbard-like bands as well as the formation of a new, empty O 2p band. The presence of an empty O 2p band is a unique feature representing the presence of 2DEG at the LAO/STO heterointerface.

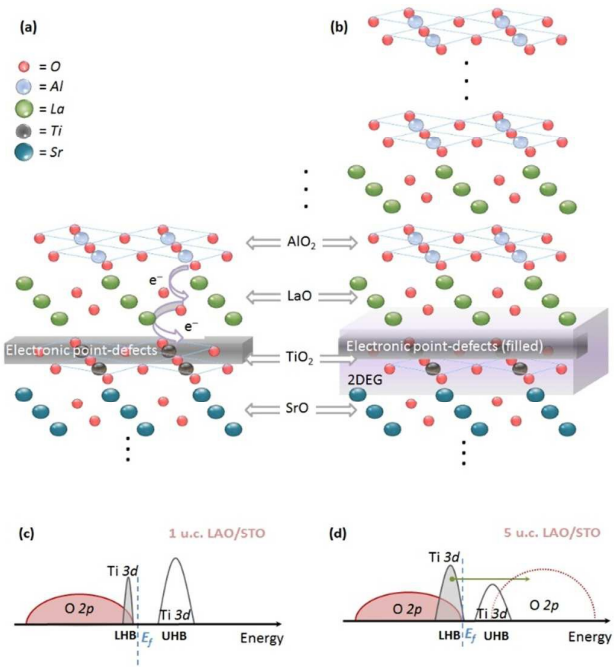

Fig. 8. Layered representation for 1 u.c. (a) and 5 u.c. (b) $LaAlO_3/SrTiO_3$ samples and electronic band diagram for insulating (c) and conducting (d) samples. Mechanism of electron transfer and representation of band diagram are proposed based on the O K-edge X-ray absorption near-edge spectroscopy analysis.

Based on high-energy optical conductivity measurements, a new interface transition occurs at a photon energy between 11-15 eV [14], which matches well the energy of peak 2 and the separation between the LHB and a new empty O 2p band. It is worth mentioning that we do not observe shape-resonance which can be assigned to electronically active defects states transition (peak 1) in the conducting sample. This implies that 5 u.c. of LAO provide enough charge to completely fill electronically active defects states attributed earlier as noninteger valence states of Ti ions.

Conclusions

We demonstrate that a thorough investigation of O K-edge X-ray absorption spectra can be used as a reference method to probe changes in the electronic structure of complex oxide heterostructures. Oxygen K-edge absorption spectra reveal noticeable differences in the electronic structure of insulating and conducting LAO/STO samples. For the insulating case, XANES analysis provides evidence of (i) charge redistribution between LaO and TiO2 layers, (ii) electronically active defects sites, identified as noninteger valence states e.g. $Ti^{(4-x)+}$, where $0 < x < 1$ and (iii) release of accumulated negative charge presented at tSTO, e.g. electronic reconstruction. Reconstruction manifests itself mainly as charge redistribution between O 2p and Ti $^{4+}$ as well as defect-induced Ti $^{(4-x)+}$ orbitals. At these orbitals electrons are localized and have no mobility, explaining the insulating nature of 1 u.c. LAO/STO sample. For the conducting case, a new shape-resonance (peak 2) is observed, and attributed to a pronounced O 2p-O 2p interaction. These findings suggest that that charge redistribution between LaO and TiO2 layers is still in place and concentration of electronic defects increased proportionally with LaAlO3 thickness. For larger defect concentrations the electronic defect states begin to interact. The interaction between electronic defects leads to a stronger hybridization between Ti $3de_g \Leftrightarrow$ O 2p orbitals, resulting in an increased delocalization of O 2p states and in improved carrier transport. No shape-resonance, which can be assigned to noninteger valence states of Ti, is found, indicating that these states are fully populated for a LAO thickness of 5 u.c. A remaining fraction of available electrons is responsible for 2DEG formation. We also do not observe evidence of significant change in the crystallographic structure or/and cation intermixing in 1 u.c. and 5 u.c. LAO/STO samples. All differences originate from the change in electronic structure. Our result also shows that O K–edge X-ray absorption spectroscopy is sensitive to reveal new states and access degree of hybridizations at interfaces and is applicable to other oxide heterostructures.

Acknowledgements

This work is supported by Singapore National Research Foundation under its Competitive Research Funding (NRF-CRP 8-2011-06 and NRF2008NRF-CRP002024), MOE-AcRF-Tier-2 (MOE2015-T2-1-099), NUS-YIA, and FRC. We also would like extend our appreciations to Mr. Lim Chee Wai and Mr. Wong How Kwong for the technical support.

Notes and references

1 A. Ohtomo & H. Y Hwang, *Nature*, 2004, **427**, 423-426
2 Ariando, X. Wang, G. Baskaran, Z. Q. Liu1, J. Huijben, J. B. Yi, A. Annadi, A. R.Barman, A. Rusydi, S. Dhar, Y. P. Feng, J. Ding, H. Hilgenkamp and T. Venkatesan, *Nat. Commun.*, 2011, **2**, 188-194
3 J.-S. Lee, Y.W. Xie, H. K. Sato, C. Bell, Y. Hikita, H. Y. Hwang and C.-C. Kao, *Nat. Mater.*, 2013, **12**, 703-706
4 A.Brinkman, M. Huijben, M. van Zalk, J. Huijben, U. Zeitler, J. C. Maan, W. G. van der Wiel, G. Rijnders, D. H. A. Blank and H. Hilgenkamp, *Nature Mat.*, 2007, **6**, 493-496
5 D. A. Dikin, M. Mehta, C.W. Bark, C. M. Folkman, C. B. Eom, and V. Chandrasekhar, *Phys. Rev. Lett.*, 2011, **107**, 056802

6 J. A. Bert, B. Kalisky, C. Bell, M. Kim, Y. Hikita, H. Y. Hwang and K. A. Moler, *Nature Physics*, 2011, **7**, 767-771
7 S. Thiel, G. Hammerl, A. Schmehl, C. W. Schneider, J. Mannhart, *Science*, 2006, **313**, 1942
8 C. Cen, S. Thiel, J. Mannhart, & J. Levy, Science, 2009, 323(5917), 1026-1030
9 A. Ron & Y. Dagan, Phys. Rev. Lett., 2014, 112(13), 136801.
10 S. Okamoto, A. J. Millis, and N. A. Spaldin, *Phys. Rev Lett.*, 2006, **97**, 056802
11 M. Takizawa, H. Wadati, K. Tanaka, M. Hashimoto, T. Yoshida, A. Fujimori, A. Chikamatsu, H. Kumigashira, M. Oshima, K. Shibuya, T. Mihara, T. Ohnishi, M. Lippmaa, M. Kawasaki, H. Koinuma, S. Okamoto, and A. J. Millis, *Phys. Rev. Lett*., 2006, **97**, 057601
12 A. Annadi, Q. Zhang, X. Renshaw Wang, N. Tuzla, K. Gopinadhan, W.M. Lu, A. R. Barman, Z.Q. Liu, A. Srivastava, S. Saha, Y.L. Zhao, S.W. Zeng, S. Dhar, E. Olsson6 B. Gu, S. Yunoki, S. Maekawa, H. Hilgenkamp, T. Venkatesan and Ariando, *Nature Commun*.,2013, **4**, 1838
13 N. Nakagawa, H.Y. Hwang, and D. A. Mueller, *Nat. Mater*., 2006, **5**, 204-209
14 T.C. Asmara, A. Annadi, I. Santoso, P.K. Gogoi, A. Kotlov, H.M. Omer, M. Motapothula, M.B.H. Breese, M. Ruebhausen, T. Venkatesan, Ariando and A. Rusydi, *Nature Commun*., 2014, **5**, 3663
15 N. Pavlenko, T. Kopp, E. Y. Tsymbal, J. Mannhart and G.A. Sawatzky, *Phys. Rev. B*, 2012, **86**, 064431
16 A. Kalabukhov, R.Gunnarsson, J. Börjesson, E. Olsson, T. Claeson and D.Winkler, *Phys. Rev. B*, 2007, **75**, 121404(R)
17 R. Pentcheva and W. E. Pickett, *J. Phys.: Condens. Matter*, 2010, **22**, 043001
18 J. Cazaux, *J. Electron Spectrosc. Relat. Phenom*., 1999, **105**, 155-185
19 B. Gilbert, R. Andres, P. Perfetti, G. Margaritondo, G. Rempfer and G. de Stasio . *Ultramicroscopy*, 2000, **83**, 129-139
20 Agarwal, B. K. X-ray Spectroscopy-An Introduction, Springer-Verlag (1991)
21 X. Yu, O. Wilhelmi, H. O. Moser, S. V. Vidyaraj, X. Gao, A. T. S. Wee, T. Nyunt, H. Qian, H.Zheng, J. *Electron Spectrosc. Relat. Phenom.*,2005, **144–147**, 1031-1034
22 G. Ertl and J. Kueppers, Low Energy Electrons and Surface Chemistry, VCH, (1985)
23 F.M.F. de Groot, J. *Electron Spectrosc. Relat. Phenom*., 1993, **62**, 111-130
24 Z. Ristic, R. Di Capua, G. M. De Luca, F. Chiarella, G. Ghiringhelli, J. C. Cezar, N. B. Brookes, C. Richter, J. Mannhart and M. Salluzzo, *EPL*, 2011, **93**, 17004
25 G. van der Laan. *Phys. Rev. B*, 1990, **41**, 12366
26 M. Kawasaki, K.S. Takahashi, T. Maeda, R. Tsuchiya, M. Shinohara, O. Ishiyama, T. Yonezawa, M. Yoshimoto, H. Koinuma, *Science*, 1994, **266**, 1540
27 G. Koster, B.L. Kropman, G.J.H.M. Rijnders, D.H.A. Blank, H. Rogalla, *Appl. Phys. Lett.*,1998, **73**, 2920
28 G. Koster, G. Rijnders, D.H.A. Blank, H. Rogalla, *Physica C*, 2000, **339**, 215
29 T. Ohnishi, K. Shibuya, M. Lippmaa, D. Kobayashi, H. Kumigashira, M. Oshima, H. Koinuma, *Appl. Phys. Lett*., 2004, **85**, 272
30 T. Kubo, H. Nozoye, *Phys. Rev. Lett.*, 2001, **86** 1801
31 S. A. Chambers , T.C. Droubay, C. Capan, G.Y. Sun, *Surface Science*, 2012, **606**, 554–558
32 D. C. Qi, A.R. Barman, L. Debbichi, S. Dhar, I. Santoso, T. C. Asmara and A. Rusydi, *Phys. Rev. B.*, 2013, **87**, 245201
33 S.Kumar, S. Gautam, G.W. Kim, F. Ahmed, M.S. Anwar, K.H. Chae, H.K. Choi, H. Chung, B.H. Koo, *Applied Surface Science*, 2011, **257**, 10557-10561
34 M. Onoda, *Journal of Solid State Chemistry,* 1998, **136(1)**, 67-73
35 C. N. R. Rao, S. Ramdas, R. E. Loehman & J. M. Honig, *Journal of Solid State Chemistry*, 1971, **3(1)**, 83-88
36 M. W. Ruckman, Jie Chen, S. L. Qiu, P. Kuiper and M. Strongin, *Phys. Rev. Lett*.,1991, **67**, 2533-2536
37 P. K. Gogoi, L. Sponza, D. Schmidt, T. C. Asmara, C. Diao, J. C. W. Lim, S. M. Poh, S.Kimura, P. E. Trevisanutto, V. Olevano and A. Rusydi, *Phys. Rev. B.*,2015, **92**, 035119